Vacancy-type defect production in CLAM steel under He and H ion beams implantation studied with positron-annihilation spectroscopy

Yong Xin[1] Xin Ju[1*] Jie Qiu[2] Liping Guo[3] Tiecheng Li[3] Fengfeng Luo[3] Peng Zhang[4], Xingzhong Cao[4] Baoyi Wang[4]

[1]Department of Physics, University of Science and Technology Beijing, Beijing, 100083, P. R. China

[2] Nuclear Engineering Program, The Ohio State University, Columbus, Ohio 43210, USA

[3]Accelarator Laboratories, School of Physics, Wuhan University, Wuhan, Hubei 430072, P. R. China

[4]Key Laboratory of Nuclear Analysis Techniques, Institute of High Energy Physics, Chinese Academy of Sciences, Beijing 100049, P. R. China

Corresponding author: Tel.: +86-10-62333921; Fax: +86-10-62333921; E-mail: jux@ustb.edu.cn

Abstract

The vacancy-type defects induced by co-implantation of He and H ions in China Low Activation Martensitic (CLAM) steel at room temperature were investigated with a variable-energy position beam Doppler broadening spectra (DBS). The co-implantation contained two patterns: one was implanted by He ions firstly, and then followed by H-ions implantation; the other was implanted by H ions in the first place, after that followed by He-ions implantation. The S parameters of implanted samples became larger than un-implanted one under different implantation fluences, and the S parameters of pre-implanted H were larger than pre-implanted He regardless of fluence. The difference of S parameters between pre-implanted H and He decreased with increasing fluence. He-H-vacancy complex is the reason that the S parameter of pre-implanted H is higher than pre-implanted He.

Keywords: positron annihilation, ion implantation, vacancy-type defects, CLAM steel

1. Introduction

Reduced-Activation Ferritic/Martensitic (RAFM) steels are candidate materials for the structural components of a fusion reactor because of their excellent resistance to radiation damage, high thermal conductivity and low thermal expansion coefficient compared with austenitic steels [1,2]. China Low Activation Martensitic (CLAM) steel is one of RAFM steel which has been studied by a number of institutes and universities in China [3,4]. One of the critical issues for the application of F/M steels is the effect of He and H produced by nuclear reactions (n, p) and (n, α). Much attention is given to the effect of He and H in materials during the development of fusion energy sources in view of their negative influence on the radiation resistance of structural materials[5,6]. He has low solubility in metals and they will be trapped by vacancies, vacancy complexes and grain boundaries. He is essentially immobile at temperatures below $0.4T_m$ and participates strongly in cavity nucleation and stabilization [7]. The stabilization of cavities by He, resulting in void swelling, has been reported at temperatures from 350°C to 700°C [8]. H exhibits a much higher solubility in steel accompanied by a relatively low binding energy to simple lattices [9,10]. In specimens implanted with H alone, H will quickly diffuse away from the implanted area at moderate temperatures. Below 100°C, some H is weakly trapped by radiation-induced defects, in a depth profile greatly broadened from the calculated initial profile [11].

He and H have different interaction with irradiation induced defects, it is important to investigate the synergistic effect among He, H and defects. The

synergistic effect of He and H has been investigated by TEM [12], but TEM has its resolution limit to investigate the defects. For this reason, Positron annihilation spectroscopy is an effective method to detect the defects which cannot be observed by TEM. Positron annihilation spectroscopy (PAS) [13] is one of the more powerful and well-established techniques to characterize vacancy-type defects [14] (micro-voids and open volume regions) of a material. Since positively charged nuclei are absent at vacancy-type defects, positrons are trapped and annihilate there with the surrounding electrons, conveying the information on the local electronic environment around the vacancy-type defects. This technique provides a highly sensitive penetrative probe combining the sensitivity of positrons to defects with the penetrability of gamma rays. Lifetime, Doppler broadening and coincidence Doppler broadening measurement have been used to study defects of metals [15,16,17,18] and nonmetal [19,20]. Doppler broadening is an effective way to detect the vacancy-type defects after ion beam irradiation [21], so this method could be used to the field of nuclear materials which will be irradiated high energy beams in fission or fusion reactors.

In our work, PAS was used to analysis the defect profile of CLAM steel after co-implantation of He and H ions. In our previous work [17,22], He-ion and co-implantation of He and H ions were performed at fixed sequence with different fluencies to investigate the evolution of defects. Therefore, the implanted fluence was main variable. In this paper, the synergistic effect of He, H and defects will be discussed. For this reason, co-implantation of He and H ion were performed at different sequence to investigate the interaction among the three. Compared with our

previous work, the implanted sequence and the discussed topic are different.

2. Experiment

The CLAM steel was produced by University of Science and Technology Beijing. The steel was reaustenitized at 960°C for 0.5h and air cooling, and then it was tempered at 760°C for 1.5h and air cooling, with the cooling rate is on 10°C/s [23]. The normalized temperature is different from our previous work [17, 22]. The detailed compositions used in this study are shown in Table.1 [23]. The size of implanted samples is 10×10×1.5mm^3 cut from CLAM steel, afterwards surfaces of samples were polished by sandpaper and diamond paste, respectively.

Table 1

Chemical composition of material studied (wt. %)

Material	Cr	W	V	Ta	C	Mn	Fe
CLAM	9.08	1.48	0.18	0.097	0.098	0.46	Bal

Co-implantation was carried out at room temperature with 200keV ion accelerator located in the Accelerator Lab of Wuhan University. The dimensions of beam is 20×20mm^2 and beam current density is 0.75μA/cm^2. Thermocouples are mounted at the surface of the specimen to measure the specimen surface temperature. The increment of temperature during implantation is less than 5°C according to the measurement. The energy of He and H ions were 140keV and 80keV, respectively. The co-implantation contains two parts: the first part is that He ions were implanted firstly, and then followed by H-ion implantation; the second one is opposite to the first, which means that H ions were implanted first of all, followed by He-ions implantation.

The fluence at the sample is measured by a current intergrator and detailed fluences of implantation are shown in Table.2. All of them are accumulative fluences.

Table.2

The fluences of implantation at room temperature

Sample number	Ion	Fluence(ions/cm^2)
1	He	1e+15
	H	5e+15
2	H	5e+15
	He	1e+15
3	He	5e+15
	H	2.5e+16
4	H	2.5e+16
	He	5e+15
5	He	1e+16
	H	5e+16
6	H	5e+16
	He	1e+16

Positron beam measurements were performed at room temperature with a variable energy slow positron beam at the Key Laboratory of Nuclear Analysis Techniques, Institute of High Energy Physics, Chinese Academy of Sciences[24 , 25]. Monoenergetic positrons in the energy range 0.1keV-20keV were implanted into the sample. The implanted positrons rapidly thermalize and then diffuse until they annihilate with electrons, producing pairs of gamma ray (511keV) photons. The Doppler broadening spectra, recorded using a high-purity Ge detector (1.2keV energy resolution at the 514keV). Doppler broadening of the 511keV annihilation line was

analyzed using the S and W parameter. In brief, the value of S parameter is defined by the ratio of counts in the central energy region (511±0.8keV in this paper) of the annihilation gamma peak and the total number of counts in the peak. The value of W parameter is defined as the ratio of the wing area (504.2-508.4keV and 513.6-517.8keV in this paper) to the total number of counts in the peak. Vacancy-type defects induced by ion implantation act as trapping sites for positrons, which results in a greater contribution to the central region corresponding to an increase in the S-parameter.

3. Results

The optical micrograph of CLAM steel is shown in Fig.1, which indicates the microstructure is lath-type martensite.

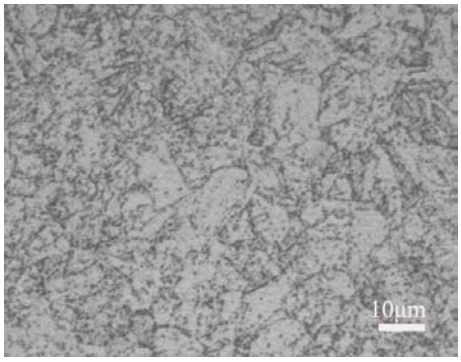

Fig.1 Optical micrograph of CLAM steel

Fig.2 shows the dependence of the S parameter on implanted positron energy (S-E curve) for co-implantation at different fluences. The top x-axis of Fig.2 is the mean depth of the annihilating positrons. The detailed fluences are marked in figure. For un-implanted sample, the S parameter decreases rapidly from 0.4613 at positron energy is 0keV to 0.4440 at 2.5keV, and then decreases slowly with increasing positron energy and approaches 0.4268 at 20keV for bulk annihilation. All the samples were polished by sandpaper and diamond paste before implantation. The polishing procedure generates plastic region which contains high density of

dislocation [26]. Positron can be trapped by dislocation, but it is a shallow trap for positron. When the density of dislocation reaches $10^{9}cm^{-2}$, the S parameter will be constant if the density increased sequentially [27]. The density of dislocation of RAFM steel is on $10^{10}cm^{-2}$ [28], so the influence of dislocation on S parameter in our experiment is limited. The vacancy-type defects induced by following implantation will be detected by positron and induce the increase of S parameter. Therefore, the defects induced by polishing can be neglected. The S parameter of implanted sample became larger than that for un-implanted one, which indicates that positrons detect the presence of vacancy-type defects generated during implantation, regardless of the fluence. The S parameter curves exhibit a broad maximum around positron beam energy of 9keV (170nm) for all the implanted samples, and then gradually decreases with increasing positron energy. For the two implanted patterns, the fluences of He and H were the same, but the implanted sequence is different. Fig.2 indicates that the S parameters of pre-implanted H are larger than pre-implanted He for all the fluences, but the difference of S parameters between the two implanted patterns decreases with increasing fluence.

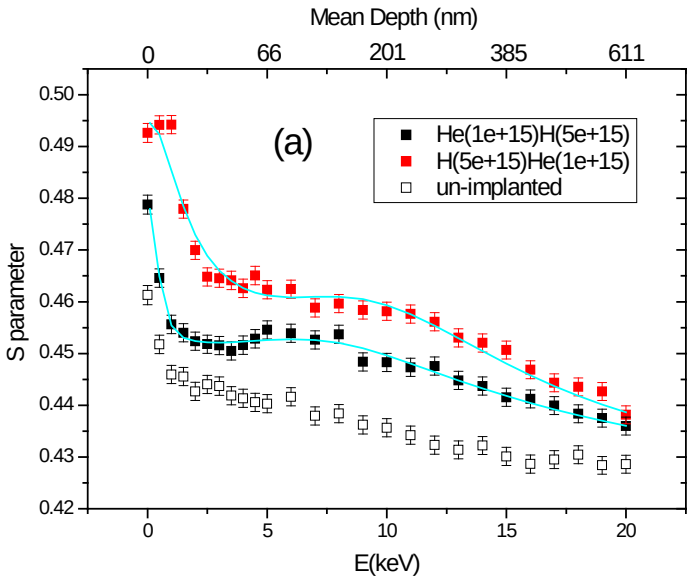

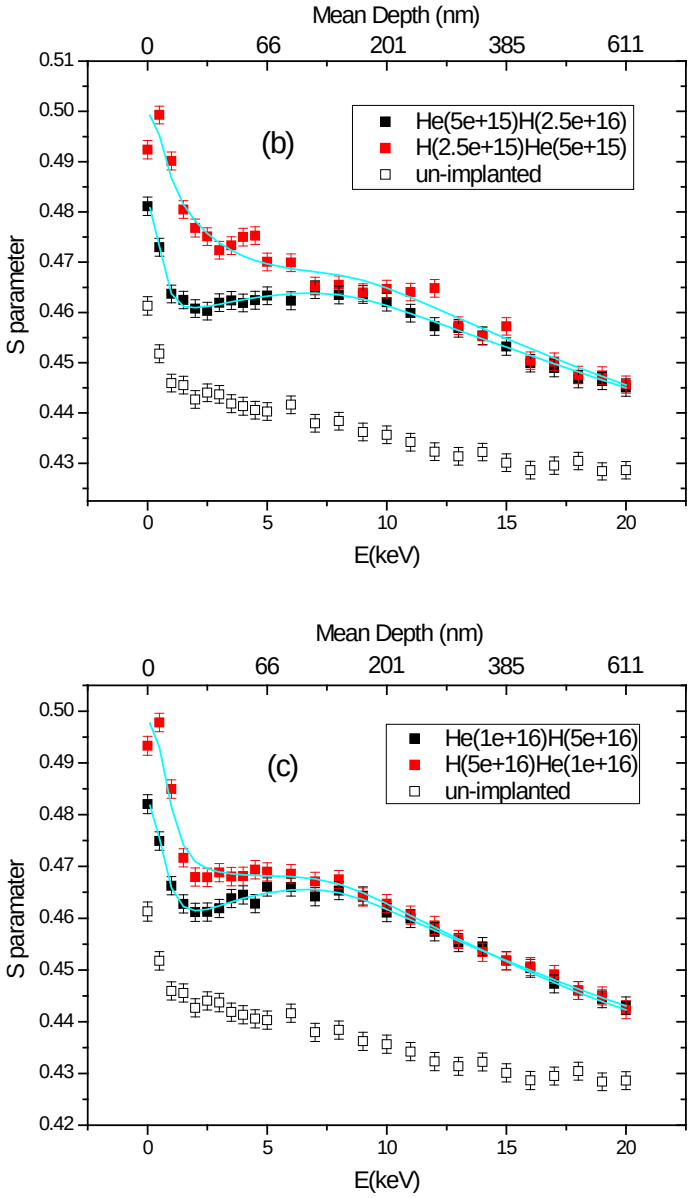

Fig.2 S-E curves of implanted samples

The S parameter data as a function of the mean depth were fitted in a multi-layer model using a computer program VEPFIT [29].The fitted S parameter of bulk value is 0.4269±0.0002 and the effective positron diffusion length in bulk is 120±8nm. In our work, four-layer models obtained agreement between experiment and model for post-implanted samples. The thickness of each layer, normalized S parameter (normalized to bulk S parameter) and diffusion length of positron in each layer are plotted as function of depth, shown in Fig.3. In this figure, the first and fourth layers are surface and bulk layers, respectively, and the rest two are implanted layers. The defects are located mainly in the two implanted layers, so the S parameters of the two

layers are discussed in this work. In the following discussion, the two implanted layers are marked as S^1_{irr} and S^2_{irr} layers in order to discuss conveniently. The fitted results show that the value of S^1_{irr} is larger than S^2_{irr} for all the samples, which is in accordance with the maximum value of S parameter at 170nm as the boundary of S^1_{irr} is about 300nm.

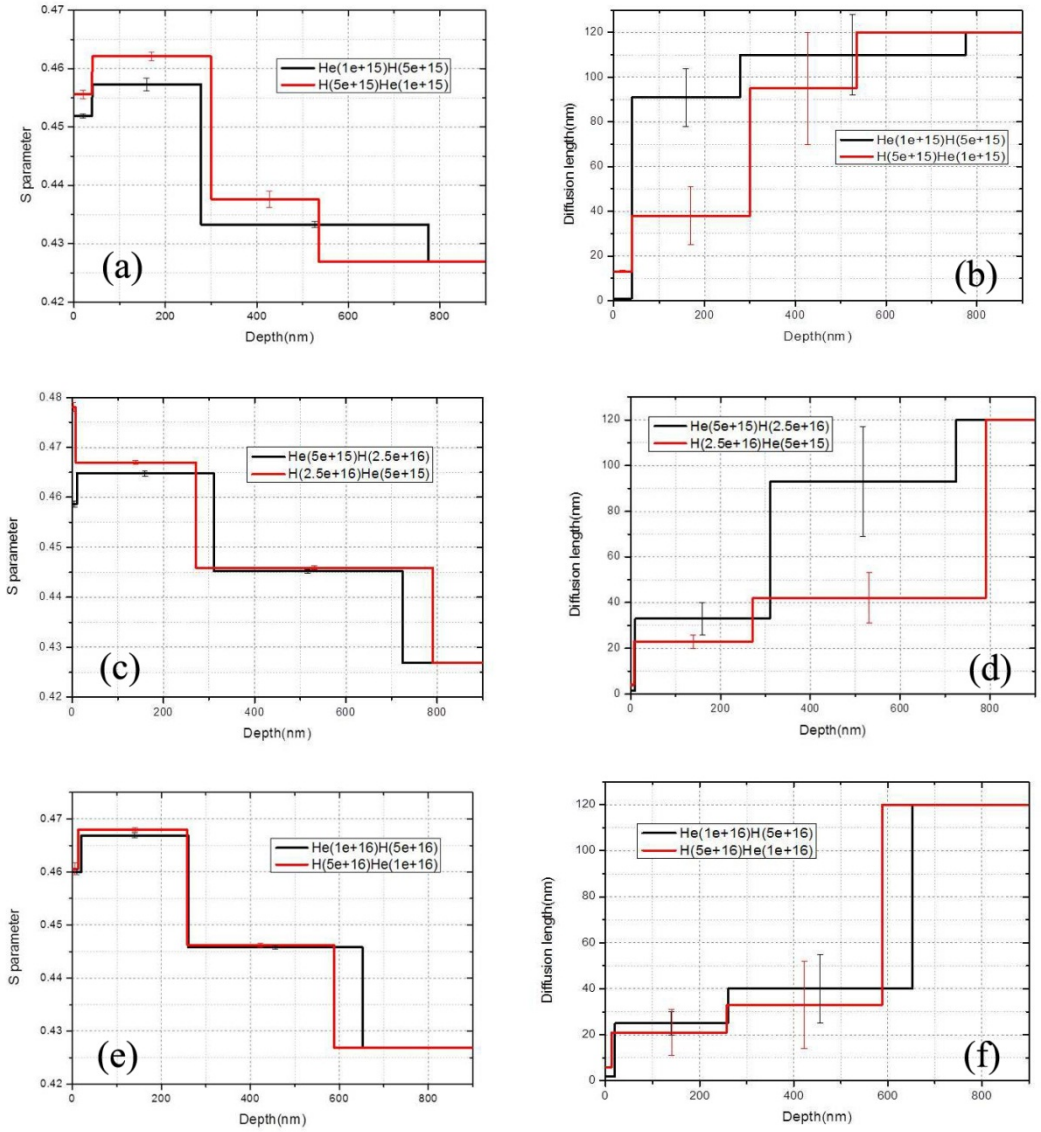

Fig.3 Fitted result of implanted samples

4. Discussion

4.1 Calculated results of SRIM

The dependence of the S parameter on depth is relative with the distribution of vacancy-type defects in sample, so the distribution of defects is discussed firstly.

SRIM [30] calculation gives the distribution of implanted ions and defects, shown in Fig.4. In our calculation, the Fe, Cr, W, V, Mn and Ta were added to target according to their real content shown in Table.2 and the density is 7.848g/cm^3. The displacement energy is 40eV and the lattice binding energy is 2eV [31, 32, 33]. The surface binding energy is defaulted value for each element in SRIM calculation. The distribution of vacancies induced by 140keV He and 80keV H are shown in Fig.4, and the distribution of implanted ions are shown, too.

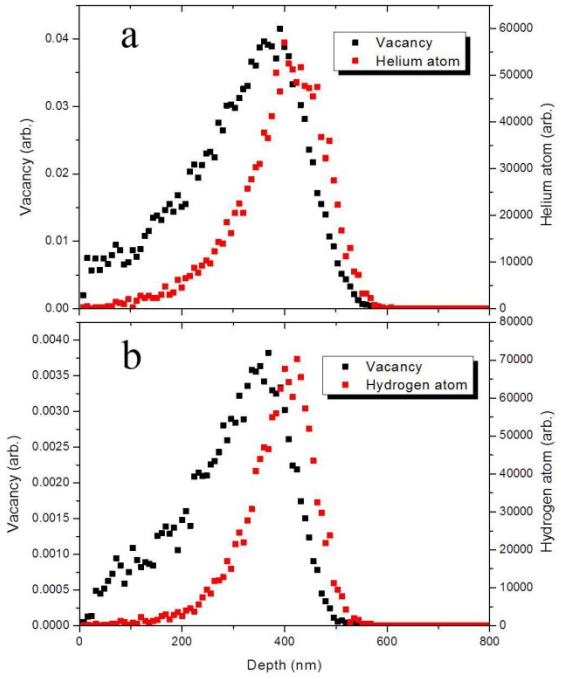

Fig.4 Distribution of ions and vacancies

Fig.4 indicates that the peak value of the two implanted ions and generated vacancies are the same. SRIM could give the final distribution of ions projected on XY, XZ and YZ planes, which are shown in Fig.5. The X is the depth axis; Y and Z axis are orthogonal with X axis. In this figure, a, b and c are the XY longitudinal, XZ longitudinal and YZ lateral distribution of He ions, respectively; d, e and f are the corresponding results of H ions. The projected range, lateral range and radial range of the two ions are shown in Table.3. The straggle of every parameter is shown in this table too.

Table.3 The projected range, lateral range and radial range of 140keV-He and 80keV-H

		Range (nm)	Straggle (nm)
140-keV He	Projected	386.3	88.4
	Lateral	92.5	115.2
	Radial	146.4	72.9
80-keV H	Projected	381.5	72.4
	Lateral	77.2	96.3
	Radial	120.7	62.3

Here, projected range is the mean projected range of all ions on the X-axis, which means that most of ions located at this depth; the lateral range and radial range reflect the distribution of ions on Y and Z-axis, the straggle is the square root of the variance. The data in Table.3 indicated that most of He and H ions are located at same depth, but the spatial distribution of He ions is wider than H ions, which can be shown in Fig.5, too. For co-implantation, the post-implanted ions and generated vacancies are overlapping with pre-implanted ones. Therefore, all the implanted ions and generated vacancies would interact with each other. The defects induced by co-implantation will be discussed in the following part.

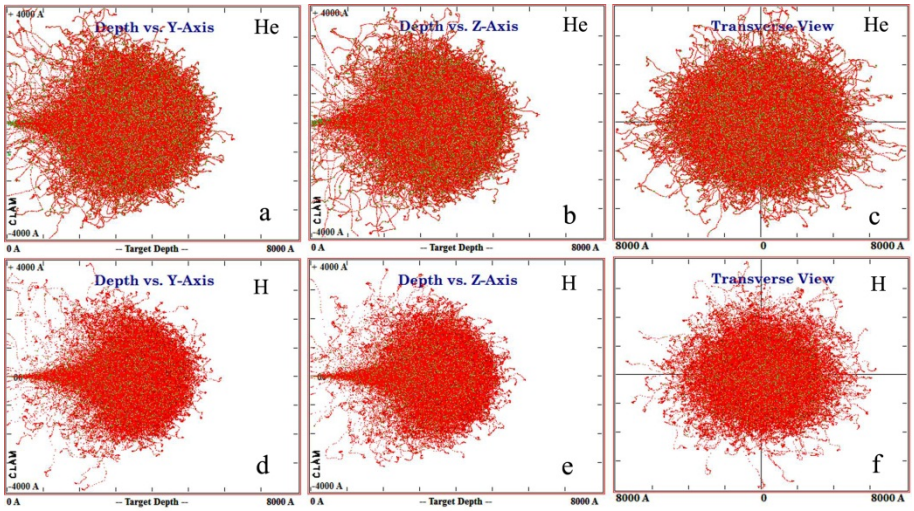

Fig.5 Distribution of ions projected at different planes

4.2 The kinds of vacancy-type defect and their effect for S parameter

Irradiation-induced mono-vacancies can ba migrate in the 260-460K range in steel [34], so they can aggregate to form vacancy-clusters at room temperature. He atoms

have strong binding energy with vacancy and vacancy-cluster [35,36]. Therefore, He-vacancy complex are formed after He implantation. The de-trapping energy of He atom form He-vacancy complex changes from 2.7 to 3.5eV according to the number of He atom and vacancy in complex[37]. Therefore, the He-vacancy complex is stable at room temperature. Thermal helium desorption behavior could certify this conclusion, too [38]. First principle calculation showed that vacancy is strong sink to trap hydrogen [39], so H-vacancy complex is existed after hydrogen implantation. However, the binding energy between H and vacancy is weak and H-vacancy complex decomposes at room temperature [40]. Positron annihilation lifetime spectra showed that hydrogen induced defect is vacancy cluster of 5-7 vacancies at room temperature [41]. For mixed-beam implantation, vacancy cluster, He-vacancy and H-vacancy complexes are existed vacancy-type defects regardless of implanted sequence.

Firstly, the S parameters of S^1_{irr} and S^2_{irr} for every implanted sample are discussed. Fig.4 indicates that both the implanted atoms and vacancies locate at 300-500nm mainly, which is corresponding to the S^2_{irr} region. Because the binding energy between He atom and vacancy is strong, He-vacancy complex are located in S^2_{irr} region mainly. Compared with S^2_{irr} region, the amount and distribution of He atom in S^1_{irr} region are smaller and wider, respectively, which are shown in Fig.4 and Fig.5. Therefore, vacancy-clusters can be formed in this region. When positrons are trapped at vacancy-type defects coupled with He, the value of S parameter is lower than that of vacancy-type defects [42]. For this reason, the S parameters of S^2_{irr} region are

smaller than S^1_{irr} for all the samples.

Secondly, the difference of S parameters between pre-implanted He and H are discussed. Both the S parameters of S^1_{irr} and S^2_{irr} for pre-implanted H are larger than pre-implanted He for all samples. For pre-implanted H, the quick diffusion of H atoms and weak binding energy between H atom and defect make the depth profile of defects and H atoms broaden from the calculated initial profile [11]. Therefore, the vacancies generated by H diffused into deeper depth and located closer to post-implanted He atoms. The post-implanted He could trap the vacancies induced by themselves and H ions to form more He-vacancy complexes, and the complex is main defect for pre-implanted H. For pre-implanted He samples, He-vacancy clusters are formed in advance, and then vacancies brought by post-implanted H were trapped by residual He atoms which did not combine with vacancies during He implantation. Although the binding energy between H and defects is weak, H is trapped more stably in the He-associated trapped sites [43], so the post-implanted H were trapped by He-vacancy complex to form He-H-vacancy cluster. Compared with the defects of pre-implanted H, H in He-H-vacancy clusters could degrade the trap capacity of positron more severely [44]. Therefore, the S parameter of pre-implanted He is smaller than pre-implanted H.

The difference between the S parameters decreases with increasing fluence. With the increase of fluence, the amount of implanted ions increased, too. TEM results indicated that He bubble did not form when the influence of He reaches $5\times10^{20}cm^{-2}$ at room temperature [45]. Annealing experiment of irradiated steel showed that He

bubble formed when temperature was higher than 723K [46]. Compared with our experiment, both the influence and temperature are smaller. So He bubble did not form at high fluence and the defects are still vacancy-type defects at high influence. For pre-implanted H, density of defects induced by H-ion irradiation increased with increasing fluence, which reflected by diffusion length of positron in Fig.3. These defects could be stabilize by post-implanted He atoms to be the cores to absorb vacancies introduced by following He irradiation to develop into micro-voids. Although micro-voids formed at high fluence will make the S parameter increas, He atoms in them will make the S parameter decrease. The two processes made the increase of S parameter limited. For pre-implanted He, more vacancies were generated by post-implanted H with increasing fluence. So vacancies could aggregate to form vacancy-clusters in addition to that trapped by He atoms, and these vacancy-clusters made the increment of S parameter. Therefore, the difference of S parameter values between pre-implanted He and H becomes smaller with increasing fluence.

5. Conclusion

The defect profiles in CLAM steel after implantation with 140 keV He ions, 80 keV H ions at different fluences at room temperature were observed using positron-annihilation spectroscopy. The S parameters are larger for pre-implanted H than pre-implanted He. The difference of S parameters between pre-implanted H and He decreases with increasing fluence. Vacancy-clusters, He-vacancy, H-vacancy and He-H-vacancy complex are existed defects after implantation. H in He-H-vacancy

complex makes the S parameters of pre-implanted He be smaller than pre-implanted H.

Acknowledgement

This work was supported by a grant from the Major State Basic Research Development Program of China (973 Program) (No.2008cb717802) and the National Natural Science Foundation of China (No.11075119).

References

[1] R.L. Klueh, D.S. Gelles, S. Jitsukawa, A. Kimura, G.R. Odette, B. van der Schaaf, M. Victoria. J. Nucl. Mater. 307-311 (2002) 455-465.

[2] Jinnan Yu, Qunying Huang, Farong Wan. J. Nucl. Mater. 367-370 (2007) 97-101.

[3]Y. Li, Q. Huang, Y. Wu, T. Nagasaka, T. Muroga. J. Nucl. Mater. 367-370 (2007) 117.

[4] Fei Zhao, Jiansheng Qiao, Yina Huang, Farong Wan, Soumei Ohnuki. Mater. Charact. 59 (2008) 344.

[5] A. Hasegawa, M. Ejiri, S. Nogami, M. Ishiga, R. Kasada, A. Kimura, K. Abe, S. Jitsukawa. J. Nucl. Mater. 386-388 (2009) 241-244.

[6] C. Liu, H. Klein, P. Jung. J. Nucl. Mater. 335 (2004) 77-82.

[7] I. Mukouda, Y. Shimomura, T. Iiyama, J. Nucl. Mater. 283-287 (2000) 302.

[8] J. D. Hunn, E. H. Lee, T. S. Byun, L. K. Mansur. J. Nucl. Mater. 282 (2000) 131-136.

[9] K.L. Wilson, in: Data Compendium for Plasma-Surface Interactions, Nuclear Fusion Special Issue 1984, International Atomic Energy Agency, Vienna, 1984, pp. 28-42.

[10] M.B. Lewis, K. Farrell, in: F.W. Wi.en, J.A. Spitznagel (Eds.), Advanced Techniques for Characterizing Microstructures, AIME, New York, 1982, p. 487.

[11] J.D. Hunn, M.B. Lewis, E.H. Lee, in: AccApp 98- Proceedings of the Second International Topical Meeting on Nuclear Applications of Accelerator Technology, American Nuclear Society, La Grange Park, 1998, p. 375.

[12]T. Tanaka, K. Oka, S. Ohnuki, S. Yamashita, T. Suda, S. Watanabe, E. Wakai. J. Nucl. Mater. 329-333 (2004) 294-298.

[13] P. Hautojarvi, A. Dupasquier, et. al, Positrons in Solids, Sprinqer-Verlaq, New York, 1979.

[14] P.J. Schultz, K.G. Lynn, Rev. Mod. Phys. 60 (1988) 701.

[15] Hamdy F.M. Mohamed, Junhyun Kwon, Yong-Min Kim, Whungwhoe Kim. Nucl. Instr. Meth. Phys. Res. B, 258 (2007) 429-434

[16] J. Kwon, H.F.M. Mohamed, Y.M. Kim, W. Kim. Nucl. Instr. Meth. Phys. Res. B, 262 (2007) 255-260

[17] J. Qiu, Y. Xin, X. Ju, L.P. Guo, B.Y. Wang, Y.R. Zhong, Q.Y. Huang, Y.C. Wu. Nucl. Instr. Meth. Phys. Res. B, 267 (2009) 3162-3165.

[18] E.E. Abdel-Hady. Nucl. Instr. Meth. Phys. Res. B, 221 (2004) 225-229.

[19] Dongyun Wan, Baoyi Wang, Chunlan Zhou, Chuangxin Ma, Yutian Wang, Rengang Zhang, Long Wei. Physica B 344 (2004) 489-494.

[20] M. Fujinami, R. Suzuki, T. Ohdaira, T. Mikado. Appl. Surf. Sci. 149(1999)188–192.

[21] T. Iwai, Y. Ito, Mater. Sci. Forum 445&446 (2004) 120.

[22] J. Qiu, X. Ju, Y. Xin, S. Liu, B.Y. Wang. J. Nucl. Mater. 411(2011)20-24.

[23] J. Qiu, X. Ju, Y. Xin, S. Liu, Y.L. Wang, H.B. Wu, D. Tang. J. Nucl. Mater. 407 (2010) 189-194

[24] P. Wang, X.Z. Cao, Y.Y. Ma, X.B. Qin, B.Y. Wang, C.X. Ma, L. Wei. HEP&NP 30 (2006) 1036-1040 (in Chinese)

[25] X.Z. Cao, B.Y. Wang, Z.M. Zhang, C.F. Wei, T.B. Zhang, D.S. Xue, L. Wei. Nucl. Sci. Tec 27 (2004) 435-439 (in Chinese)

[26] F. Klocke, O. Dambon, G.G. Capudi Filho. Wear 258 (2005) 1794–1803

[27] Y.C. Wu, Y.C. Jean. Applied Surface Science 252 (2006) 3278–3284

[28] R Schäublin, P Spätig, M Victoria. J. Nucl. Mater. 258-263 (1998) 1178-1182

[29] A. van Veen, H. Schut, J. de Vries, R.A. Hakvoort, M.R. Ijpma, AIP Conf. Proc. (218) (1991) 171 – 198.

[30] J.F. Ziegler, J.P. Biersack, U. Littmark, The Stopping and Range of Ions in Solids, Pergamon, New York, 1985. http://www.srim.org.

[31] P. Jung. Phys. Rev. B. 23 (1981) 664

[32] J. Nucl. Mater. 417 (2011) 1013-1017

[33] J. Nucl. Mater. 318 (2003) 241-248

[34] C. Dimitrov, M. Tenti, O. Dimitrov, J. Phys. F Met. Phys. 11 (1981) 753.

[35] C.J. Ortiz, M.J. Caturla, C.C. Fu, F. Willaime, Phys. Rev. B. 75 (2007) 100-102.

[36] Chu-Chun Fu, F. Willaime, Phys. Rev. B. 72 (2005) 064117.

[37] K. Morishita, R. Sugano, B.D. Wirth, J. Nucl. Mater. 323 (2003) 243 – 250.

[38] X.Z. Cao, Q. Xu, K. Sato, T. Yoshiie. J. Nucl. Mater. 417 (2011) 1034 – 1037.

[39] W.A. Counts, C. Wolverton, R. Gibala. Acta Mater 58 (2010) 4730-4741

[40] S. Linderoth, A.V. Shishkin, Philos. Mag. A 55 (3) (1987) 291.

[41] Y.Q. Chen, Y.C. Wu, Z. Wang, S.J. Wang. Radiation Physics and Chemistry 76 (2007) 308 – 312

[42] S.V. Naidu, S. Gupta, A. Sen, P. Mukhopadhyay, G. Bhandari, R.K. Bhandaric, P.

Sena, Radiat. Eff. Defect. Solid. 83 (1984) 29 – 134.

[43] Masahiko Ogura, Norisuke Yamaji, Tetsuya Higuchi, Makoto Imai, Akio Itoh, Nobutsugu Imanishi, Kiyotomo Nakata, Nucl. Instr. Meth. Phys. Res. B. 136-138 (1998) 483-487.

[44] K. Kiuchi, R.B. McLellan, Acta Metall. 31 (1983) 961

[45] J. Nucl. Mater. 367-370 (2007) 500-504

[46] A. Kimura, R. Kasada, R. Sugano, A. Hasegawa, H. Matsui, J. Nucl. Mater. 283–287 (2000) 827–831